Journal of
Marine Science and Engineering

MDPI

Article

Spatial Distribution and Decadal Variability of ^{129}I and ^{236}U in the Western Mediterranean Sea

Maria Leimbacher [1], Lorenza Raimondi [1,*], Maxi Castrillejo [2], Christof Vockenhuber [3], Habacuc Pérez-Tribouillier [1,3], Katrin Schroeder [4], Toste Tanhua [5] and Núria Casacuberta [1,3,*]

1 Institute of Biogeochemistry and Pollutant dynamics (IBP), Department of Environmental Systems Science, ETH Zürich, 8092 Zürich, Switzerland; mleimbacher@student.ethz.ch (M.L.)
2 Institute of Earth Sciences (ISTE), Faculty of Geosciences and Environment, University of Lausanne, 1015 Lausanne, Switzerland
3 Laboratory of Ion Beam Physics, Department of Physics, ETH Zürich, 8093 Zürich, Switzerland
4 CNR-ISMAR Istituto di Scienze Marine, Consiglio Nazionale delle Ricerche, 30122 Venezia, Italy
5 GEOMAR Helmholtz Centre for Ocean Research, 24148 Kiel, Germany
* Correspondence: lorenza.raimondi@usys.ethz.ch (L.R.); nuria.casacubertaarola@usys.ethz.ch (N.C.)

Abstract: This study investigates the spatial and temporal distribution of the artificial radionuclides ^{129}I and ^{236}U in the Western Mediterranean Sea, focusing on their connection to radionuclide sources and circulation dynamics. Taking advantage of unprecedented precision of accelerator mass spectrometry, both tracers were firstly investigated in 2013. Here, we examine tracer observations obtained along four stations (re-)visited during the *TAlPro2022* expedition in May 2022. Distributions of both ^{129}I and ^{236}U were related to water masses and clearly linked to local circulation patterns: a tracer-poor surface Atlantic inflow, a thining of the tracer minimum at intermediate depths, and a higher tracer signal in Western Mediterranean Deep Waters due to dense water formation in the Algero-Provençal basin. The comparison to 2013 tracer data indicated recent deep ventilation of the Tyrrhenian Sea, the mixing of deep waters and enhanced stratification in intermediate waters in the Algero-Provençal basin due to a temperature and salinity increase between 2013 and 2022. We estimate an overall ^{129}I increase of 20% at all depths between 0 and 500m with respect to 2013, which is not accompanied by ^{236}U. This suggests either the lateral transport of ^{129}I from the Eastern Mediterranean Sea, or an additional source of this tracer. The inventories of ^{129}I calculated for each water mass at the four stations point to the deposition of airborne releases from the nuclear reprocessing plants (La Hague and Sellafield) on the surface Mediterranean waters as the more likely explanation for the ^{129}I increase. This work demonstrates the great potential of including measurements of anthropogenic radionuclides as tracers of ocean circulation. However, a refinement of the anthropogenic inputs is necessary to improve their use in understanding ventilation changes in the Mediterranean Sea.

Keywords: ^{236}U; ^{129}I; tracer; artificial radionuclides; Mediterranean Sea; atmospheric source

Citation: Leimbacher, M.; Raimondi, L.; Castrillejo, M.; Vockenhuber, C.; Pérez-Tribouillier, H.; Schroeder, K.; Tanhua, T.; Casacuberta, N. Spatial Distribution and Decadal Variability of ^{129}I and ^{236}U in the Western Mediterranean Sea. *J. Mar. Sci. Eng.* **2024**, *12*, 2039. https://doi.org/10.3390/jmse12112039

Academic Editor: Gianluca Quarta

Received: 9 September 2024
Revised: 4 November 2024
Accepted: 5 November 2024
Published: 11 November 2024

1. Introduction

The ocean plays a key role in regulating Earth's climate system through the redistribution and storage of heat and gases in its interior. This process is primarily driven by dense water formation (i.e., ventilation), which only occurs in limited regions of the world's ocean [1]. Similarly to the global ocean, the Mediterranean Sea displays regions of active deep water formation (Figure 1, blue circles); however, this process occurs here at a faster pace and with a high spatial and temporal variability [2]. The easily accessible deep water formation sites in the Mediterranean Sea and the rapid time of water turnover (about ten times shorter than in the global ocean), allows for the detailed observation and measurement of circulation patterns of one of the most ventilated water bodies [3–5]. Because of its circulation processes and its rapid response to global warming, studies

identify the Mediterranean Sea as a potential "miniature ocean laboratory" suitable to better understand the global ocean's response to climate change and a valuable tool to predict future scenarios [4–6].

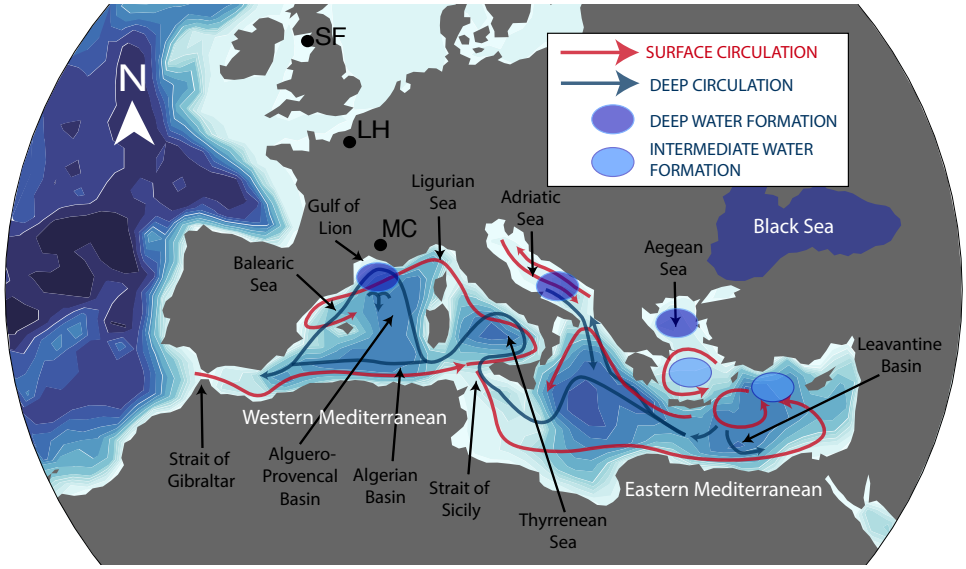

Figure 1. Map of the Mediterranean Sea with locations of nuclear reprocessing plants (black dots), and arrows of surface (red) and deep (blue) circulation pathways. Locations of deep (dark blue circles) and intermediate water (light blue circles) formation are also shown here. SF = Sellafield; LH = La Hague; MC = Marcoule.

1.1. Circulation and Water Masses of the Study Area

The Mediterranean Sea is a mid-latitude, semi-enclosed sea connected to the Atlantic Ocean through the narrow Strait of Gibraltar, where water, salt, heat and other properties are exchanged between the basins (Figure 1). The Mediterranean Sea is composed of two basins of similar size (i.e., a Western and an Eastern Basin; WMED and EMED), connected by the Sicily Channel [7]. Circulation within the Mediterranean Sea, as described in more detail in e.g., Millot [2], is schematically divided into three circulation cells; a shallow inter basin circulation as well as two deep overturning cells, located each in the WMED and the EMED. The upper branch of the inter basin circulation cell is occupied by Atlantic Water (AW) entering the Mediterranean Sea at surface and flowing eastwards while increasing in salinity and density due to net evaporation (Figure 1, red arrows). The lower branch of the inter basin circulation cell is represented by the Levantine Intermediate Water (LIW), which forms in the Levantine basin and from there flows back westwards between 200 and 600 m and eventually outflows into the Atlantic Ocean through the Strait of Gibraltar (Figure 1). The transit time of LIW from the formation region to the Gulf of Lion is estimated to be around 10 years (y) [2]. The second circulation cell is characterized by the formation of the Eastern Mediterranean Deep Water (EMDW) in the EMED, mainly in the Adriatic Sea by Bora winds. In a similar manner, deep water is formed in the Gulf of Lion in the WMED, which represents the third circulation cell. Regional cold and dry winds, Mistral and Tramontane, lead to rapid cooling of the AW and strong evaporation, which triggers convection of AW and its mixing with underlying, warmer and saltier LIW finally forming the Western Mediterranean Deep Water (WMDW). Further, another intermediate water is the Western intermediate water (WIW), only formed in case of moderate deep convection (if the AW only mixes with LIW but not with WMDW [2,8]). Yet, deep water formation in the Mediterranean Sea shows strong temporal variability. An example is the intense deep water formation event observed between 2004–2006 which marked the beginning of the Western Mediterranean Transition (WMT; [9]). This deep water formation event was preconditioned by dry and cold winters and persistent winds in the Gulf of Lion, which led to a near-complete renewal of the WMDW within two years throughout the whole western

basin (i.e., Ligurian Sea, Balearic Sea, and Algerian basin) [10,11]. A second climatological event, known as the Eastern Mediterranean Transient, occurred in the 80/90s and deeply affected the circulation in the EMED by shifting deep water formation from the Adriatic to the Aegean Sea. This strong deep water formation determined an uplift of Ionian deep waters and consequently affected the characteristics of waters in the WMED [11,12].

1.2. Artificial Radionuclides as Tracers of Water Masses

Circulation pathways and timescales, including mixing and advection, can be tracked using unreactive, soluble chemical compounds released into the marine environment with time-dependent input functions (i.e., transient tracers). The most commonly used transient tracers in ocean studies are the man-made chlorofluorocarbons (CFCs) and sulphur hexafluoride (SF_6) [13]. However, in recent years and owing to the advancements in accelerator mass spectrometry (AMS), artificial radionuclides iodine-129 (^{129}I) and uranium-236 (^{236}U) have emerged as new and powerful oceanic tracers, as discussed in Casacuberta and Smith [14] and references therein. These are long-lived tracers (half-life $T_{1/2}$ = 15.7 My and $T_{1/2}$ = 23.5 My, respectively) conservatively transported by oceanic currents due to their inertness. Whereas ^{129}I has been widely used as an oceanographic tracer since 1980 (e.g., [15–17]), ^{236}U measurements were enhanced more recently through technological improvements in compact AMS systems [18]. Further, ^{129}I has a potential to act like a proxy due to its long half-life and provide information about partitioning of other shorter lived radionuclides of radiological concern such as ^{131}I (half-life $T_{1/2}$ = 8 d) [16]. Both ^{129}I and ^{236}U have been emitted into the atmosphere and subsequently, or directly, into the oceanic mixed layer by nuclear bomb tests occurring between 1945 and 1980 as well as by nuclear accidents such as Fukushima and Chernobyl [16,19]. Nuclear Fuel Reprocessing Plants (NFRPs) further contributed to the presence of these radionuclides in the ocean. Among these, the two largest facilities are located in La Hague (France) and Sellafield (Great Britain). Unlike the atmospheric input from global fallout, NFRPs are point-like sources. These facilities mostly discharge liquid radioactive waste that is transported lateraly by ocean dynamics [20], and a much smaller airborne fraction [21] that is often overlooked in oceanographic studies.

In the last decade, the combination of ^{129}I and ^{236}U has emerged as a novel tool for ocean circulation studies with a growing number of investigations that have unveiled new pathways of water masses, their provenance and mixing, and estimated circulation transit times in the Arctic Ocean and the Nordic Seas [14,22,23].

1.3. ^{129}I and ^{236}U in the Mediterranean Sea

A first basin-wide study of ^{129}I and ^{236}U was conducted in 2013 by Castrillejo et al. [24], which provided useful benchmark values of radionuclide concentrations, and the first quantitative estimates of radionuclide sources in the Mediterranean Sea. The study of Castrillejo et al. [24] added to prior studies that measured a single depth profile of ^{236}U in the Ligurian Sea (Station DYFAMED; see Figure 2) in 2001 [25] and 2013 [26] and others that provided ^{129}I concentrations in surface waters off the Rhône estuary [27,28]. Yet, these studies already pointed to the limitation of using ^{129}I and ^{236}U as transient tracers in the Mediterranean Sea, due to poor understanding of their local sources and historical releases (input functions). Unlike in the Arctic Ocean, where the major source of these tracers is their liquid release from NFRPs, the main input of ^{129}I and ^{236}U to the Mediterranean Sea is global fallout (1 kg and 11 kg of ^{129}I and ^{236}U released in the basin, respectively) and the nuclear reprocessing plant of Marcoule (a total accumulation of 70–90 kg and 10–20 kg for ^{129}I and^{236}U, respectively). Artificial radionuclides released by Marcoule (MC in Figure 1) were introduced into Mediterranean waters through atmospheric deposition and direct discharges via the Rhône River [29]. On the other hand, the influence of the Chernobyl nuclear accident (1986) on tracers' distribution was found to be negligible in the region, since deposition of ^{236}U occurred primarily in the vicinity of the accident area, and ^{129}I was dispersed primarily to the North (not affecting the Mediterranean Sea) [30]. However, the study of Castrillejo

et al. [24] reported concentrations of both artificial radionuclides that would suggest an additional source to the Mediterranean Sea (e.g., atmospheric contribution of the active NFRPs of La Hague and Sellafield), but concluded that further data would be necessary to validate such conclusion.

Here, we present a new study in the Western Mediterranean Sea that investigates ^{129}I and ^{236}U distributions using a selection of new data collected during the *TAlPro2022* expedition in May 2022. This study only covers 4 of the 24 hydrographic stations, which correspond to the ones previously occupied during a GEOTRACES expedition in May–June 2013 (Figure 2). The overarching goals of this study are to (1) better constrain the spatial distribution of ^{129}I and ^{236}U along the water column and in prominent water masses of the WMED; and (2) assess the decadal changes in the tracers' concentration and distribution between 2013 and 2022. We discuss the results in the context of their general input history, with a focus on constraining new sources of radionuclides and whether these are observed in the deep waters formed in the WMED. This is a very first step towards the determination of input functions in the region, which are essential for future precise assessment of water age through transit time distribution models.

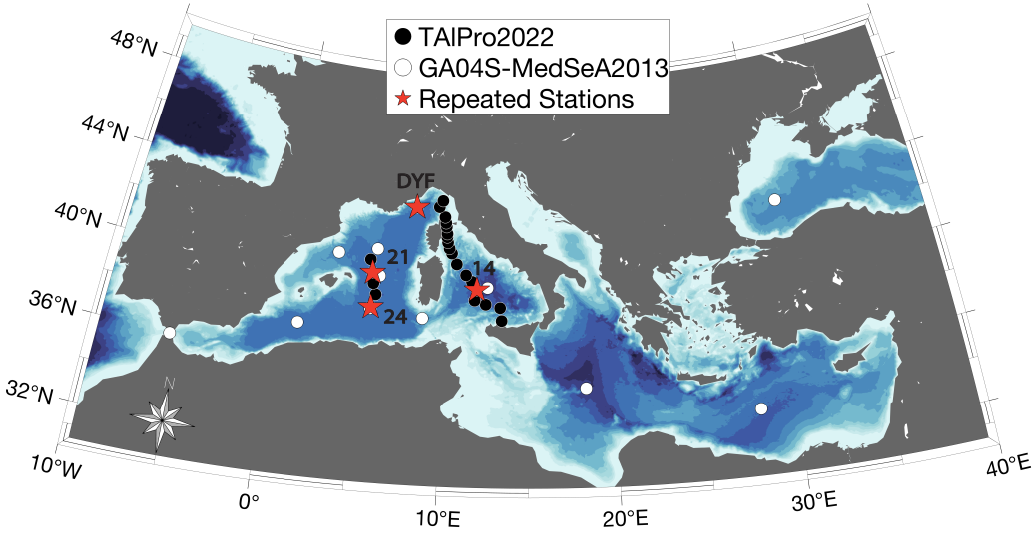

Figure 2. Map of the Mediterranean Sea with locations of the stations sampled for ^{129}I and ^{236}U in 2013 as part of the GA04S-MedSeA2013 expedition (white circles); and in 2022 during the TAlPro2022 cruise (black circles). The four stations discussed in this work were sampled during both expeditions and are marked as red stars (with name of stations reported; DYF = DYFAMED).

2. Materials and Methods

2.1. Sampling for Artificial Radionuclides

The *TAlPro-2022* cruise was conducted in the framework of the Med-SHIP program [31] and thanks to a trans-national access project funded by the EUROFLEETS+ European Project. The cruise took place on board of the *RV Belgica* (from Toulon to La Spezia) in May 2022 and covered 24 hydrographic stations in the WMED along a north–south transect from the Ligurian Sea to the Tyrrhenian Sea as well as 5 sites west of Sardinia in the Algero-Provençal basin (Figure 2). These stations revisited sites that were previously sampled for ^{236}U, ^{129}I or both radionuclides (red stars in Figure 2). Stations 14, 21 and 24 were first sampled in 2013 during the *GEOTRACES GA04S-MedSeA* expedition [24]. The fourth is the so-called DYFAMED station, which was previously sampled for ^{236}U in 2001 and 2013 [25,26]. During the *TAlPro-2022*, seawater was collected at each station from 15–17 depths doubling the depth resolution of 2013. The seawater was collected using Niskin bottles mounted on a rosette equipped with sensors for conductivity, temperature, and depth (CTD). At the repeated stations, 3 L of seawater (total fraction, i.e., not filtered)

were collected in plastic cubitainers and stored at dark and room temperature conditions until further extraction of ^{236}U and ^{129}I in Zürich.

2.2. Extraction and Measurements of ^{129}I and ^{236}U

The isotope isolation and measurement was conducted at ETH Zürich based on the methods adapted by Casacuberta et al. [32] and described in more detail in Wefing et al. [33] and Christl et al. [34]. Briefly, for the extraction of ^{129}I, about 250 mL of seawater were spiked with 1.5 mg of Woodward Iodine (WWI; ^{127}I). The amount of ^{127}I added to each sample is about 3 orders of magnitude more than the natural amount in seawater (i.e., 60 ppb), thus the only purpose of adding it is to account for the chemical losses of ^{129}I, and to obtain measured atomic ratios of $^{129}I/^{127}I$ in the order of 10^{-12}. After letting the spike equilibrate with the sample, the aliquots were oxidized to iodate using saturated $Ca(ClO)_2$ solution, then reduced to iodide using $Na_2S_2O_5$ and NH_2OH*HCl. The reaction mixture was raised to pH 5–6 before passing through a preconditioned DOWEX 1 × 8 ion exchange resin to purify and retain the iodine. Then, 2.25 M KNO_3 was used to elute the iodine into an acidified $AgNO_3$ solution and it was precipitated as AgI. The precipitate was dried, mixed with Ag powder and pressed into cathodes for AMS measurements.

The processing of ^{236}U consists of a pre-concentration and a purification step. In short, seawater samples of 3 L were acidified using 3 mL of concentrated HNO_3 (25%) and spiked with 1 pg of ^{233}U (acidic solution, PTB 2014-1126). Then, $Fe(OH)_3$ (equivalent of ∼250 mg of Fe^{3+} solution) was added to the sample and precipitated as Fe_2O_3 using concentrated NH_4OH solution. The Fe_2O_3 precipitate was redissolved in 8 M HNO_3 and passed through UTEVA columns to purify U. The extracted U was co-precipitated with Fe_2O_3 and thermally oxidized to UO. The extracted U was co-precipitated a final time with $Fe(OH)_3$ (equivalent of 3 mg of Fe^{3+}) and a few drops of NH_4OH. Finally, the precipitate was mixed with Nb powder and pressed into AMS cathodes.

Processed samples were measured at the Laboratory of Ion Beam Physics (LIP) at ETH Zürich using the 300 kV Multi-Isotope Low Energy AMS (MILEA) system [35]. The final ^{129}I and ^{236}U concentrations were calculated from the $^{129}I/^{127}I$, $^{233}U/^{238}U$ and $^{236}U/^{238}U$ atom ratios by multiplying it with the known amount of WWI (^{127}I) or ^{233}U spike added during the isotope extraction procedure and subtracting the concentration of the blanks [36].

2.3. Data Processing and Quality Control

During processing, each batch of ^{129}I and ^{236}U samples (n = 12 in total) included one blank (milliQ-water), processed as a sample and used to assess data quality and quantify uncertainties.

For ^{129}I, four replicates of an internal standard (a large sample collected in deep Atlantic waters) were processed in different batches to check the reproducibility of the method, resulting in a mean concentration of 1.3×10^8 at kg^{-1} and a standard deviation of 2.7%. Nevertheless, we here include a larger uncertainty that accounts for all the replicates of such internal standard throughout the whole year of measurement (mean concentration 1.9×10^8 at kg^{-1}). Therefore, we included 5% as the final uncertainty for all ^{129}I results. Blanks of ^{129}I (mean of 1.9×10^6 at kg^{-1}) were 1.5–2 orders of magnitude lower than the concentrations in seawater samples. Measurements were normalized with 11 in-house standard "C2 diluted", which resulted in a correction of 1.1 (i.e., all standards measured at (91 ± 2)% of the nominal value). A final quality check was performed once results were plotted as profiles and within the hydrographic context of temperature and salinity, as well as by comparing it with other tracers. In the particular case of ^{129}I, we identified 6 samples with results that were not consistent with the rest of the parameters (marked in Table A2 with "*"), which we have excluded from the results and discussion (i.e., not plotted in figures). Most probably these samples had analytical issues during the radiochemistry steps that could be related to the weight of the WWI spike or errors in noting the final volume of seawater analyzed.

For the normalization of the $^{236}U/^{238}U$ ratios, the in-house ZUTRI standard was measured approximately every six samples [35]. A total of 12 ZUTRI standards were measured, yielding an average correction factor of 1.4, (i.e., all standards measured at (70 ± 1)% of the nominal value). The blank contribution for ^{236}U was 0.075 ± 0.056 × 10^6 at kg^{-1} (n = 7), and represented less than 1% of the total ^{236}U content in the samples. The analysis of the blanks also allowed for a detection limit of 0.7 × 10^6 at kg^{-1} to be established, which was calculated as 3 times the standard deviation of the blank average. The final total propagated uncertainty of 3% for the ^{236}U concentrations accounts for measurement error, standard normalization, blank correction, ^{233}U spike concentration, and sample weighing. For quality control of the U data, the ^{238}U concentrations obtained by AMS were compared to those calculated using the salinity-^{236}U relationship for the Mediterranean Sea proposed by Pates and Muir [37] (see Appendix A). All our results clustered between 3.4 and 3.8 µg kg^{-1}, which is within the expected values for the Mediterranean Sea and thus indicate good accuracy of the AMS measurements. As a final measure for quality control, the $^{235}U/^{238}U$ relation of all samples was monitored to verify that values did not drift away from the natural value.

2.4. Water Masses Definitions and Column Inventory Calculations

In order to understand the vertical and spatial tracer distribution, the water masses of each location and depth are identified with the help of potential temperature (θ) and salinity. The identification is conducted by applying these hydrographic properties in thermodynamic diagrams known as T-S or θ-S diagrams, and adopting previously defined values in the literature [8,38,39]. The main water masses in the WMED are the AW, the intermediate waters (LIW and WIW), the WMDW, and the TDW. Ranges of values for these water masses are based on literature and provided in the Appendix A (Table A1).

Column inventories of ^{129}I and ^{236}U were calculated by first interpolating vertical profiles with 1m depth bin and then integrating them from surface to bottom depth or within the extent of the different water masses of the region (i.e., Surface, AW, LIW, and WMDW). The units obtained from the column inventories are atoms per square meter (at m^{-2}).

3. Results

3.1. Vertical Distribution of ^{129}I and ^{236}U in the Mediterranean Sea

Along the water column, the radionuclide concentration ranged between (7.2 ± 0.4) × 10^7 and (15.8 ± 0.8) × 10^7 at kg^{-1}, and between (11.4 ± 0.4) × 10^6 and (18.7 ± 0.3) × 10^6 at kg^{-1} for ^{129}I and ^{236}U, respectively (Figure 3, Table A2). The results exceeded natural background levels of ^{129}I (1–2 × 10^7 at kg^{-1} [16]) by one order of magnitude and ^{236}U concentrations expected from atmospheric weapon tests (6 × 10^6 at kg^{-1} [19,40]), namely global fallout (Figure 3). All results, including ^{238}U obtained from the AMS system and $^{236}U/^{238}U$ atom ratio, are displayed in Table A2, though not all are discussed below as part of the results.

Generally, both tracers showed similar trends along the water column with homogeneously mixed or increasing concentrations with depth in the shallow waters (0–300 m), followed by a strong decline and again invariant or increasing concentrations at high depths (below 2000 m, Figure 3). More specifically, ^{129}I concentrations within the first 100 m ranged between 9.8–15.7 × 10^7 at kg^{-1}. At around 100–200 m, values of ^{129}I remained constant between 100 and 300 m at around 12–13 × 10^7 at kg^{-1} that were followed by decreasing concentrations below that depth (except for station DYFAMED). Minimum concentration of 7.2–8.6 × 10^7 at kg^{-1} of ^{129}I was encountered at 1000–2250 m. ^{236}U profiles showed a similar pattern to ^{129}I (when removing the outliers at DYFAMED and Station 21, see Section 2.3 for details) (Figure 3). Surface waters contained high concentrations of ^{236}U between 12.4 and 16.2 × 10^6 at kg^{-1}, though with lower variability compared to ^{129}I. The highest ^{236}U concentrations are centered at around 100–200 m, with maximum values of 17.0–18.7 × 10^6 at kg^{-1}. Then, ^{236}U concentrations sharply dropped before they slightly

increased towards the very deep waters starting below 1000–1750 m. Recorded minimum values were 10.8–12.0 × 10^6 at kg^{-1}. The increase in very deep waters below ~1500 m for both tracers was more distinct for ^{129}I, particularly at station 24.

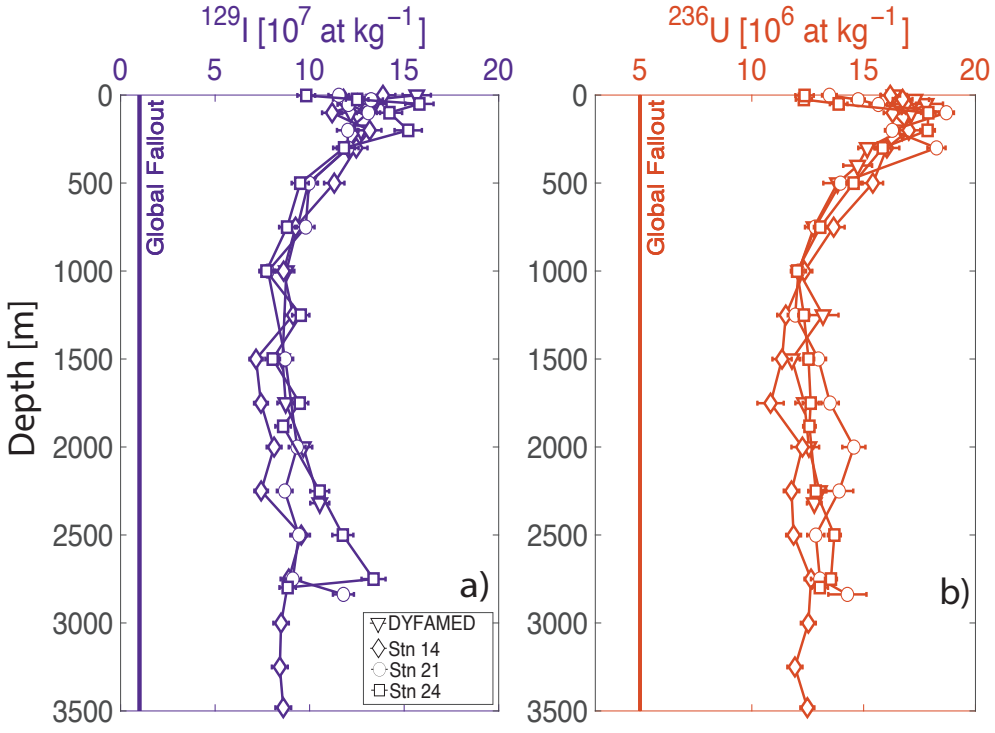

Figure 3. Vertical profiles of ^{129}I (**a**) and ^{236}U (**b**) concentrations in 2022 along the four repeated stations. Vertical lines represent values of global fallout of each tracer.

3.2. Spatial Distribution of ^{129}I and ^{236}U in the Mediterranean Sea

^{129}I showed significant variability in surface waters, ranging from 9.8 to 15.8 × 10^7 at kg^{-1}. Surface waters in the Algero-Provençal basin (stations 21 and 24), located closer to the inflow of Atlantic Water, contained lower tracer concentrations and differed more from the lower lying LIW than in the Ligurian and the Tyrrhenian Sea. While at station 24, ^{129}I increased towards the LIW reaching maximum values, the concentration of this radionuclide decreased in surface waters along the water column at DYFAMED and station 14. In general, station 24 showed the highest scatter of ^{129}I of all stations along the water column, with maximum concentrations of 15.2 × 10^7 at kg^{-1} in intermediate waters and an increase in deep water towards the seabed by 4.8 × 10^7 at kg^{-1}. In comparison, the maximum at the remaining stations was at 12.7–13.2 × 10^7 at kg^{-1}.

For ^{236}U, surface waters also showed spatial heterogeneity with values ranging from 12.4 to 16.4 × 10^6 at kg^{-1}, with lower concentrations in the Algero-Provençal basin. Concentrations of ^{236}U increased sharply between 0 and 100 m at station 24 as well as station 21 (from 12.4 to 17.9 and from 13.5 to 18.7 × 10^6 at kg^{-1}, respectively) and remained constant or only minimally increased with depth at station 14 and DYFAMED (from 16.2 to 16.3 and from 16.4 to 17.1 × 10^6 at kg^{-1}, respectively) (Figure 3). In intermediate waters, elevated values of ^{236}U were found at both station 21 and 24, with a maximum of 18.7 × 10^6 at kg^{-1} at 100 m at station 21.

3.3. ^{129}I and ^{236}U in Mediterranean Sea Water Masses

Using the water mass classification provided in Table A1, AW was found to be centered between 25 and 100 m in all four stations and characterized by temperatures of around 13.6–17.0 °C and salinities of 37.2–38.4. High tracer concentrations were found here with a mean of 12.9 × 10^7 at kg^{-1} (σ = 0.10) and of 15.7 × 10^6 at kg^{-1} (σ = 0.11) for ^{129}I

(Figure 4a) and ^{236}U (Figure 4b), respectively. In this water mass, we observed increasing concentrations with depth. In the Algero-Provençal basin, the AW showed lower uranium concentrations (12.3–15.7 $\times$ 10^6 at kg^{-1}) than in the Ligurian ($\sim$17.5 $\times$ 10^6 at kg^{-1}) and Tyrrhenian Seas ($\sim$16.5 $\times$ 10^6 at kg^{-1}). Another water mass is the LIW, whose core can be identified as a hook-like inversion in the θ-S diagrams (Figure 4). The upper boundary of LIW displayed amongst the highest concentrations of both radionuclides (station 21, 100 m: 13.1 $\times$ 10^7 at kg^{-1} ^{129}I and 18.7 $\times$ 10^6 at kg^{-1} ^{236}U). Unlike in the AW, ^{236}U concentrations in the LIW were more invariant with depth, with mean values of 13.0 $\times$ 10^7 at kg^{-1} for ^{129}I (σ = 0.11) and 16.7 $\times$ 10^6 at kg^{-1} for ^{236}U (σ = 0.07).

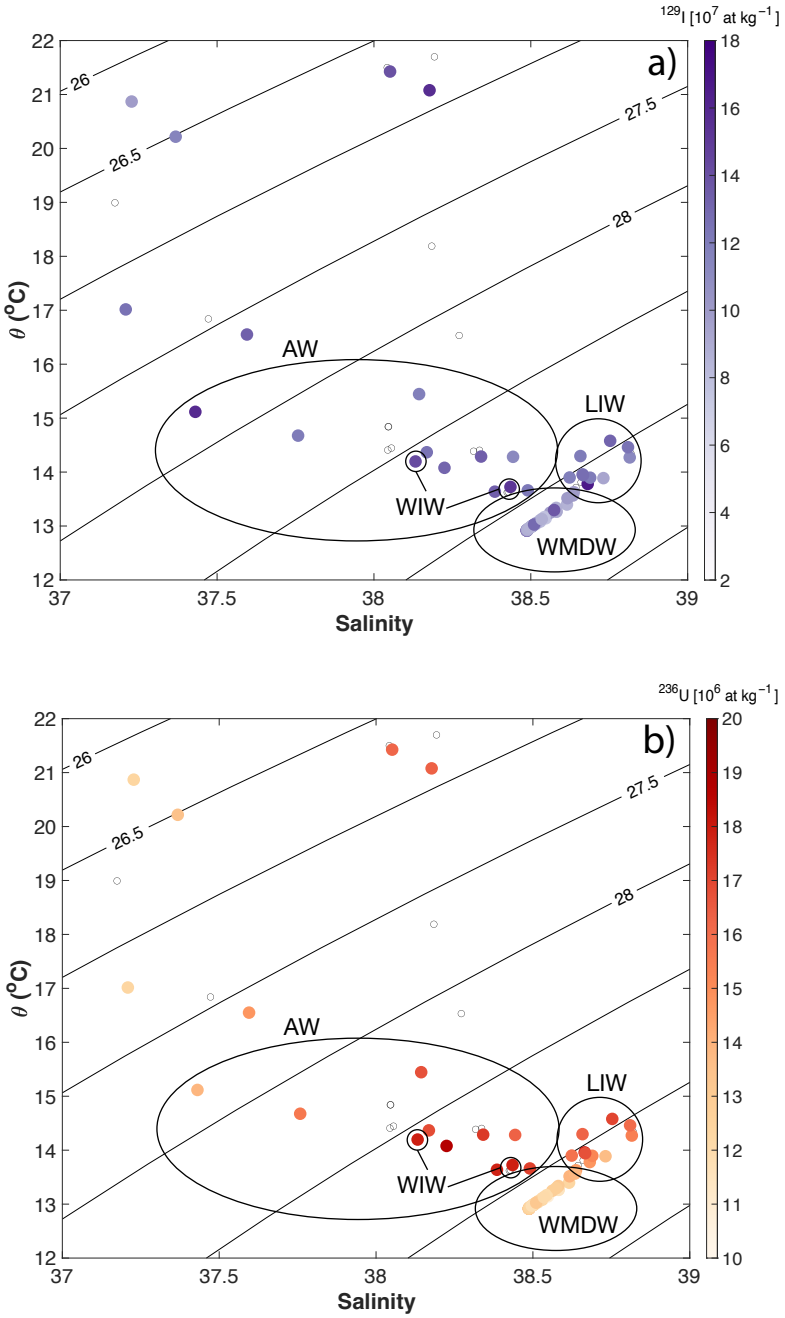

Figure 4. θ-S Diagram for the four stations of the study. Lines represent isopycnals, colours show concentrations of ^{129}I (**a**) and ^{236}U (**b**). Circles identify data within different water masses (AW = (Mediterranean) Atlantic Water; LIW Levantine Intermediate Water; WIW = Western Intermediate Water; WMDW = Western Mediterranean Deep Water). Samples in the top left side of the panel, not included in any circle, represent surface waters of Atlantic origin.

Deeper in the water column lies the WMDW, divided into new and an old components (WMDWn, WMDWo) as referring to pre- and post-WMT-event in the mid 2000s. Tracer concentrations continuously decreased with depth to a minimum of 4.3 × 10^7 at kg^{-1} for ^{129}I and 10.8 × 10^6 at kg^{-1} for ^{236}U at 1000–2250 m, depending on the station. Below that depth, increasing concentrations of both tracers were found at every station, with the highest elevation of ^{236}U at station 21 (with a 10% increase from 2500 m to bottom depth). Values ranged between 7.2–14.5 × 10^7 at kg^{-1} for ^{129}I and varied between 12.3–14.6 × 10^6 at kg^{-1} for ^{236}U. At station 14, transitional Eastern Mediterranean Deep Water (tEMDW) between 750 and 2000 m contained 8.1 × 10^7 at kg^{-1} of ^{129}I and 11.7 × 10^6 at kg^{-1} of ^{236}U, which was slightly lower than the underlying Tyrrhenian Deep Water (TDW) with mean values of 8.6 × 10^7 at kg^{-1} for ^{129}I and 12.2 × 10^6 at kg^{-1} for ^{236}U.

4. Discussion

4.1. Temporal Variability in the Western Mediterranean Sea

The results of stations 14, 21, and 24 were compared to previous ^{129}I and ^{236}U measurements of the *GEOTRACES GA04S-MedSea* expedition in 2013 [24], which are represented in Figure 2. Station DYFAMED lacked historical ^{129}I data, but had additional ^{236}U profiles collected in 2001 and 2013 [25,26]. The tracer concentrations followed similar patterns in 2013 and 2022 at all stations (Figure 5), although the depth resolution improved in 2022. The main differences to 2013 are an increase in ^{236}U concentrations in very deep waters (e.g., below 2000 m at station 21 and below 1500 m at station 14) and a decrease of 12–20% in surface waters (25 m) in the Algero-Provençal basin. On the contrary, ^{129}I increased in all locations in surface and intermediate waters between 0 and 500 m, particularly in the Algero-Provençal basin, with values going from 9.12 to 14.22 × 10^7 at kg^{-1} (station 21, 100 m). This trend was also observed in very deep waters, for example, concentrations of ^{129}I increased from 5.42 to 8.12 × 10^7 at kg^{-1} at station 14 at 2000 m between 2013 and 2022.

At DYFAMED, the ^{236}U depth profile showed drastically decreasing concentrations in surface waters (0–100 m) compared to 2001. Values decreased from 30 to 17.13 × 10^6 at kg^{-1} in surface waters and increased in deep water by about 35%. These surface concentrations highlight the effects of the NFRP Marcoule shutdown in 1997. This finding suggests that between 2001 and 2013, waters from the surface were transported by deep convection, for example, during the WMT in this decade [10], and resulted in increasing tracer concentrations in deep waters. No major renewal event similar to the WMT was observed after 2013 [41], which explains why ^{236}U concentrations below 1000 m remained constant in the last decade.

At station 24, radionuclide-rich waters transported ^{236}U deeper in the water column, thus filling the former tracer minimum observed in 2013 at 1000 m (Figure 5 station 24). Maximum ^{236}U concentrations at station 21 and 24 in 2022 were reached at 100 m compared to 250 m in 2013. Also, peaks of maximum salinity, minimum oxygen, and a decrease in temperature were situated closer to the surface in 2022 (Appendix A Figure A1).

In general, a change in both tracers and hydrographic properties indicates a variation in ocean dynamics, while a change observed only in radionuclide concentrations is referred to differences in their source(s). These two results indicate that the LIW was encountered in shallower waters already at 100 m in 2022. A possible reason is an intensified stratification of the upper layers, which prevented the LIW to further propagate into deep waters. The stratification resulted from a warming and salinification of LIW, which is especially the case for station 24, but also observed at station 21 (Figure A1). Average temperatures and salinities in AW and LIW between 100 and 500 m increased at all stations in the last decade, adding to an increase rate in salinity by +0.02–0.03 y^{-1} and in temperature by +0.06 °C y^{-1} in the Algero-Provençal basin, and lower rates of +0.01 °C y^{-1} and +0.04 y^{-1} for temperature and salinity, respectively, in the Tyrrhenian Sea (Figure A1). These trends were consistent with previously reported warming and salinification rates of LIW in the Ligurian Sea between 2007 and 2017 as a result of weakened deep convection in the Gulf of Lion in winters, after year 2014 [42]. The moderate cooling of AW and LIW in those years

changed the properties of intermediate waters, but did not result in a large production of WMDW [42].

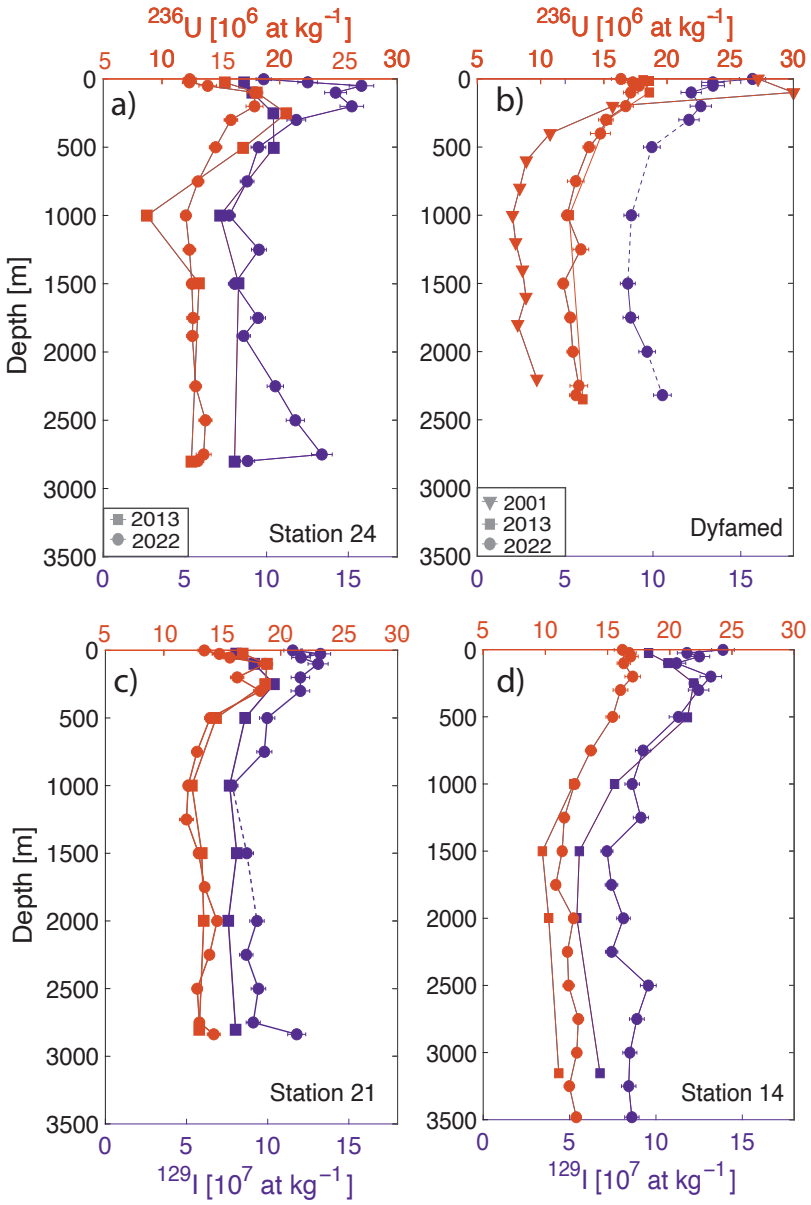

Figure 5. Depth profiles of ^{236}U (orange) and ^{129}I (purple) concentrations along four stations (panel **a**–**d**) in the Western Mediterranean Sea in 2013 and 2022 (and 2001 for DYFAMED). Note that dashed lines represent profiles shape when analytical outliers were removed.

4.2. Relative Ages of Water Masses in the Western Mediterranean Sea

As the radionuclides were not released into the environment before anthropogenic activities in the 1950s, high tracer concentrations are an indication of recently ventilated waters (i.e., young water masses). However, since we would not expect any local inputs after the shutdown of Marcoule in 1997, we should observe a decrease in concentrations both in (sub-)surface waters (AW and LIW), as well as in deeper waters (WMDW), if deep convection occurred. Both historical and recent data show overall concentrations exceeding the natural levels and global fallout signal (see Figure 3) confirming the Mediterranean Sea to be in general characterized by young water masses. Lower ^{236}U in LIW in the Tyrrhenian Sea compared to the Algero-Provençal basin suggest an increase in concentrations along the pathway of LIW in the WMED from east to west. However, this pattern cannot be

seen as clearly with ^{129}I. At station 24, we found decreasing concentrations of ^{129}I in the Ligurian Sea despite increasing water age and enhanced concentrations of LIW. The latter observation could result from the high stratification observed at this location, which indicates that the ^{129}I could be confined at this depth, unable to further propagate into deeper waters. Other possible explanations are a subduction in AW and LIW transporting the high tracer concentrations at the surface of station DYFAMED to station 24, where the elevated ^{129}I settled at deeper depths, or that the water with enhanced concentration at 100 and 200 m is WIW. This water mass probably contributed high ^{129}I from the surface into intermediate depths.

The rapid ventilation of the deep Mediterranean Sea enhances tracer concentrations close to the seabed. Above that layer, the lowest tracer concentrations in the Mediterranean Sea are found at ∼1000 m [41,43,44], a zone defined as the Tracer Minimum Zone (TMZ) by previous studies (e.g., [45]). This slow ventilated layer at mid-depths is a unique characteristic of the Mediterranean Sea and corresponds to the oldest waters in the water column [41,46]. The TMZ was observed in this study for both tracers throughout the whole WMED with the lowest concentrations in the Tyrrhenian Sea. Although the TMZ appeared to be less pronounced for radionuclides compared to gas tracers, as reported in Li and Tanhua [41], some of its patterns of distribution in the water column could still be observed.

The TDW had lower tracer concentrations than the WMDW, indicating presence of older water masses in the Tyrrhenian Sea than in other regions. This finding is consistent with that of Schneider et al. [46], who reported increasing water ages in the Tyrrhenian Sea at every depth with mean ages reaching around 100 years. Lower water ages are calculated in the Algero-Provençal basin and decrease again towards very deep waters below the centre of the TMZ at around 1000 m. Newer water from deep water formation enters the WMED in this basin, leading to enhanced ventilation and higher tracer concentrations below the TMZ [41,45]. We found increasing trends in radionuclide concentrations with depth in the Algero-Provençal basin and the Ligurian Sea starting below 1000–1750 m of ∼35% for ^{129}I and from ∼12% for ^{236}U. The increasing tracer concentrations with depth clearly indicate decreasing water ages below 2000 m compared to the upper lying waters in the TMZ. Also, higher dissolved oxygen at stations 21, 24, and DYFAMED points towards younger water masses (Appendix A Figure A1). Tracer concentrations in the deep Tyrrhenian Sea increased only slightly towards the seabed compared to the TMZ. The increase in both tracers is centered at higher depths in comparison to the other basins and is lower for the radionuclide ^{129}I. This is probably because deep water in the Tyrrhenian has different sources than the remaining basins. The upper half of the deep water (750 m–2000 m) is affected by the inflow of EMDW with high water ages and potentially low radionuclides concentrations and only the TDW below 2000 m is influenced by WMDW with higher tracer values.

4.3. Recent Ventilation of Deep Western Mediterranean Sea

In the Tyrrhenian Sea, the concentration of both tracers increased below 1000 m (Figure 5, station 14) in the last decade. At 2000m, increases from 5.42 to 8.12 × 10^7 at kg^{-1} of ^{129}I and from 10.27 to 12.28 × 10^6 at kg^{-1} of ^{236}U were observed. Concentrations were higher both in the tEMDW and the TDW. In addition, dissolved oxygen was enhanced by about 5% (from 178.9 to 186.9 µmol kg^{-1}) starting at 500 m, which indicates a ventilation of deep water in this basin in the last decade. This either occurred between 2013 and 2016 or after 2018 according to the reported intense ventilation until 2016 and declining ventilation between 2016 and 2018 by Li and Tanhua [41]. Taking both oxygen and tracer observations into consideration, one can infer that the WMT influenced the Tyrrhenian deep waters after 2013 by the entering of WMDWn in this basin, introducing newer water with higher tracer concentrations into deep layers. Similarly, increasing CFC-12 concentrations were reported from 2011 to 2016/18 [9,41] and new observations of the gas tracer SF_6 collected in 2022 also show an increase with respect to 2016 (T. Tanhua, personal communication).

In the Algero-Provençal basin, θ-S-diagrams in 2013 were characterized by inversions in waters below 2000 m [24], distinguishing between WMDWo before the WMT and WMDWn after this renewal event in the mid 2000s. In 2022, this inversion was not as distinguishable and only a minor curve is visible in the diagram below 2000 m (Figure 4), indicating that WMDWo and WMDWn mixed 17 years after the WMT (further reflected in overlapping ^{236}U concentrations in both years). Nevertheless, the slight curve of the θ-S diagram below 2000 m in 2022 aligns with enhanced ^{129}I (increase of 19% at station 21), therefore suggesting a potential increased contribution of deep waters that have been more recently ventilated and that have not undergone full mixing.

4.4. Additional Sources of ^{129}I to the Western Mediterranean Sea

Higher ^{129}I concentrations in AW and LIW in stations 21 and 24 and at surface of DYFAMED suggest a substantial recent supply of ^{129}I into the Mediterranean Sea. In order to investigate this further, column inventories were calculated for each radionuclide at every station and all years available (Figure 6). Results show an almost unchanged ^{236}U content over the past decade with increase only ranging between 0.1 to 1.2 $\times$ 10^{12} at m^{-2} (which corresponds to the inventory estimated uncertainty of 3%). Station 14 displayed a strong temporal variability in ^{236}U column inventories; nevertheless, the differences observed are an artifact due to samples only being available below 1000 m depth in 2013. When comparing the 2013 inventory to that of 2022 calculated only below 1000 m depth (brown bar chart shown in Figure 6), we still observe an increase in ^{236}U content in deep waters. Nevertheless, these findings cannot be overall conclusive in light of the lower sampling resolution of 2013.

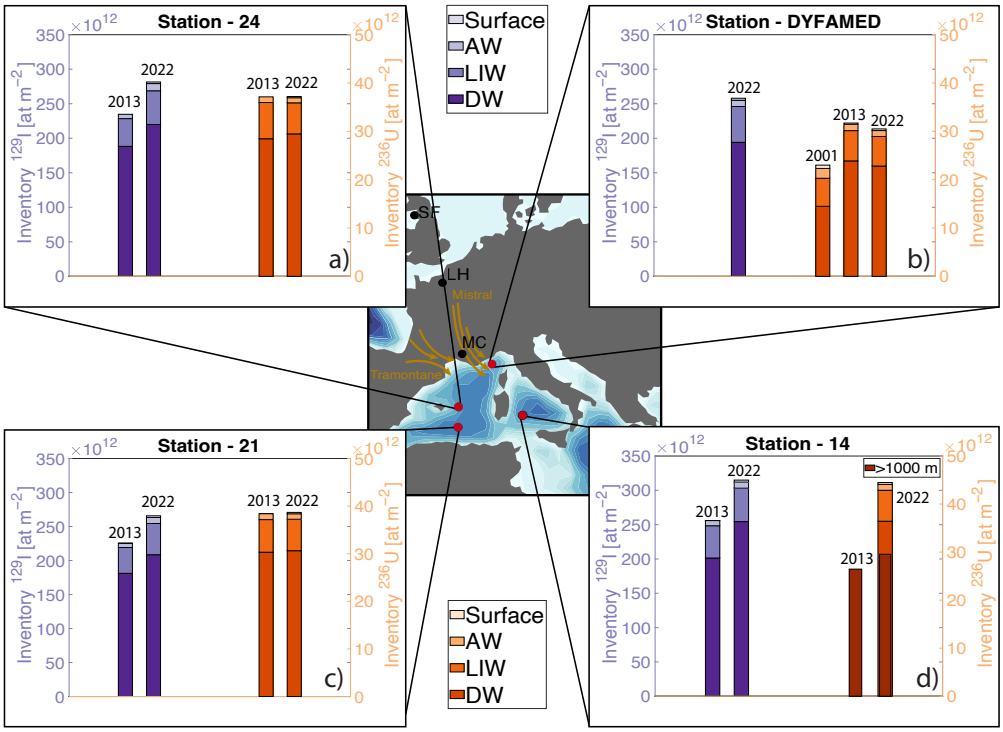

Figure 6. Column inventories of ^{129}I and ^{236}U along the four stations (panel **a**–**d**) in the WMED. The different colors of the stacked bar chart represent inventories in different water masses in the WMED for years 2013 and 2022 (when data available), and for 2001 for ^{236}U in DYFAMED. For the purpose of the figure, we used the following definitions: surface = 0–25 m; AW = 25–100 m; LIW = 100–500 m; deep water = 500 m-bottom. Note that, in 2013, ^{236}U at station 14 was only available below 1000 m so for comparison we reported inventories below this depth for 2022 as well (brown columns). The inventories uncertainty are 5% for ^{129}I and 3% for ^{236}U.

On the contrary, ^{129}I inventories increased in every station within a range of 41.1 to 80.9 $\times$ 10^{12} at m^{-2} between 2013 and 2022 (depending on the station). These values are 3 to 6 times above the 5% uncertainty estimated for the ^{129}I inventories and therefore indicate a significant increase in ^{129}I inventories over the period of observation. This increase is observed throughout the water column, yet when accounting for the percent increase of ^{129}I inventory in different water masses, we found that the highest increase occurred in the surface waters and the AW. These waters displayed an average increase of ~320% in ^{129}I inventory from 2013 to 2022, while all other layers showed a less pronounced but still remarkable percent increase that ranged between 18–65% for AW, 3–20% for LIW, and 15–25% for deep waters. In particular, stations 21 and 24 were those where the strongest increase occurred in all water masses, except the deep waters that saw the largest increase at Station 14. The observed increase in ^{129}I inventories, but the missing increase in ^{236}U, strongly suggests an additional source of ^{129}I into the WMED and particularly to the Algero-Provençal basin. Since the major increase is at surface, the most likely hypothesis points to an atmospheric source from the European NFRPs of Sellafield and La Hague. This was already pointed by other studies in the North Adriatic Sea [47], in rainwater samples collected South of Spain [48]) and was further investigated in Castrillejo et al. [24] by looking at air parcel trajectories. The latter study found that potential inputs of ^{129}I from La Hague and Sellafield would be small compared to liquid inputs from Marcoule. However, considering that Marcoule's activities already ceased 30 years ago, these new ^{129}I data clearly show that the atmospheric inputs from NFRPs could be more important than previously considered.

In fact, one could take the average surface inventory between stations 21 and 24 (5.3 $\times$ 10^{12} at m^{-2}) and a surface area of 35,500 km^2 that encompasses the Algero-Provençal stations, and estimate an average total ^{129}I inventory that could be compared to the atmospheric releases of NFRPs. When doing this calculation, we obtain a surface inventory of 1.88 $\times$ 10^{23} atoms in the Algero-Provençal basin (see Table A3 for parameters used for this estimation). Such an inventory would represent ~4% of the combined gaseous releases from La Hague and Sellafield (which was ~4.6 $\times$ 10^{24} atoms) in 2022. Mesoscale winds Mistral and Tramontane could have transported air masses over France into the Mediterranean Sea via the Rhône and the Aude valley, respectively, and deposit a substantial amount of ^{129}I, particularly to the Algero-Provençal basin. However, a more detailed study of air trajectories should be performed in order to validate these back-of-the-envelope calculations.

5. Conclusions

This study investigated the distribution of the two long-lived radionuclides ^{129}I and ^{236}U in the Western Mediterranean Sea in 2022, as well as the temporal variability in these two tracers in the last decade. Results are based on the new samples acquired during the *TAlPro2022* expedition at four repeated stations from the previous GEOTRACES cruise in 2013. The highest tracer concentrations were found in upper intermediate waters between 100 and 200 m depth and the lowest at the 1000–1750 m depth layer. Radionuclide concentrations in shallow waters were relatively low in the Algero-Provençal basin and higher in the Tyrrhenian and the Ligurian Sea. Enhanced concentrations in very deep waters were observed at most stations. Overall, the distribution of both tracers can be explained by the general circulation patterns, namely the inflow tracer-poor Atlantic Water through the Strait of Gibraltar, the westward transport of intermediate waters with high tracer concentrations, the oldest waters centered in the tracer minimum zone and finally their increase in deep and ventilated waters.

The main features of the observed temporal change in the last decade were the ventilation of the Tyrrhenian deep waters, the homogenization of Western Mediterranean Deep Waters in the Algero-Provençal basin, and the increase in heat and salt content in Levantine Intermediate Waters in the latter basin. Results also show an unexpected increase in ^{129}I inventories in surface and Atlantic waters, a feature that was not observed for ^{236}U. This finding leads to the conclusion that an additional input of ^{129}I into the Mediterranean Sea has not been accounted

for in previous studies. Based on our observations of ^{129}I inventory increase, particularly in the Algero-Provençal basin, atmospheric contributions from the nuclear fuel reprocessing plants of La Hague and Sellafield are the most likely trigger of such increase.

Since the aim of this study was to observe temporal variability in ^{129}I and ^{236}U, we here only analyzed four stations where both tracers were available; nevertheless, further regional observations of ^{129}I are available and, once measured, they will be complementary to this study, providing further insights on the circulation and evolution of the Western Mediterranean Sea at a finer resolution. Furthermore, the addition of Δ^{14}C and ventilation tracers (both measured at same stations of ^{129}I during the cruise) will provide additional information about water ages and ventilation timescales.

Author Contributions: Conceptualization, M.L., L.R. and N.C.; data curation, L.R.; formal analysis, M.L. and L.R.; funding acquisition, K.S. and N.C.; investigation, M.L.; methodology, C.V. and H.P.-T.; project administration, N.C.; resources, N.C.; supervision, L.R. and N.C.; validation, L.R., K.S., T.T. and N.C.; visualization, L.R.; writing—original draft, M.L.; writing—review and editing, L.R., M.C., H.P.-T., K.S., T.T. and N.C. All authors have read and agreed to the published version of the manuscript.

Funding: This research received no external funding, but N.Casacuberta's research is funded by the European Research Commission (ERC-2020-COG 101001451-TITANICA) and Swiss National Science Foundation (PR00P2-193091-TRACEATLANTIC).

Data Availability Statement: All new data produced for this manuscript is provided in Appendix A tables.

Acknowledgments: N. Casacuberta research is funded by the European Research Commission (ERC-2020-COG 101001451-TITANICA) and Swiss National Science Foundation (PR00P2-193091-TRACEATLANTIC). The authors want to acknowledge the support by ETHZ and the Department of Environmental Systems Science. A special thanks to K. Kündig who helped supervising M. Leimbacher in the lab and during the AMS measurements. A special thanks to Laboratory of Ion Beam Physics for the technical support during measurements. The authors would like to acknowledge the effort and dedication of the PIs, captain, officers and crew members of the *RV Belgica* during the *TAlPro2022* expedition. This cruise was possible thanks to the ship time provided by the EUROFLEETS+ Project funded by the European Commission (support given by the H2020 Grant Agreement No. 824077-EUROFLEETSPlus). Finally we would like to acknowledge the three anonymous reviewers and editor for their valuable feedback on the manuscript.

Conflicts of Interest: The authors declare no conflicts of interest.

Abbreviations

The following abbreviations are used in this manuscript:

AMS	Acceleration Mass Spectrometry
EMDW	Eastern Mediterranean Deep Water
EMED	Eastern Mediterranean Sea
EMT	Eastern Mediterranean Transient
LIW	Levantine Intermediate Water
AW	Atlantic Water
NFRP	Nuclear Fuel Reprocessing Plant
tEMDW	Transitional Eastern Mediterranean Deep Water
TDW	Tyrrhenian Deep Water
TMZ	Tracer Minimum Zone
WIW	Western Intermediate Water
WMDW	Western Mediterranean Deep Water
WMDWn	New Western Mediterranean Deep Water
WMDWo	Old Western Mediterranean Deep Water
WMED	Western Mediterranean Sea
WWI	Woodward Iodine

Appendix A

^{236}U Concentrations from ^{238}U-Salinity Relationship

^{238}U-salinity relationship of [37] is defined as:

$$[^{238}U]_{calc} = (0.0931 \pm 0.0016) \times Salinity \quad \text{(A1)}$$

^{238}U concentrations in nanograms per gram seawater (ng g^{-1}) were subsequently converted into the unit (at kg^{-1}) with the use of the Avogadro constant $N_A = 6.022 \times 10^{23}$ mol^{-1} and the molar mass of ^{238}U = 238.03 g mol^{-1}.

^{236}U in [at kg^{-1}] was then calculated by

$$[^{236}U](\text{at } kg^{-1}) = \left[\frac{^{236}U}{^{238}U}\right]_{meas} \times [^{238}U]_{calc} \quad \text{(A2)}$$

equal to the data process from AMS-results as in Section 2, solely using calculated instead of measured ^{238}U.

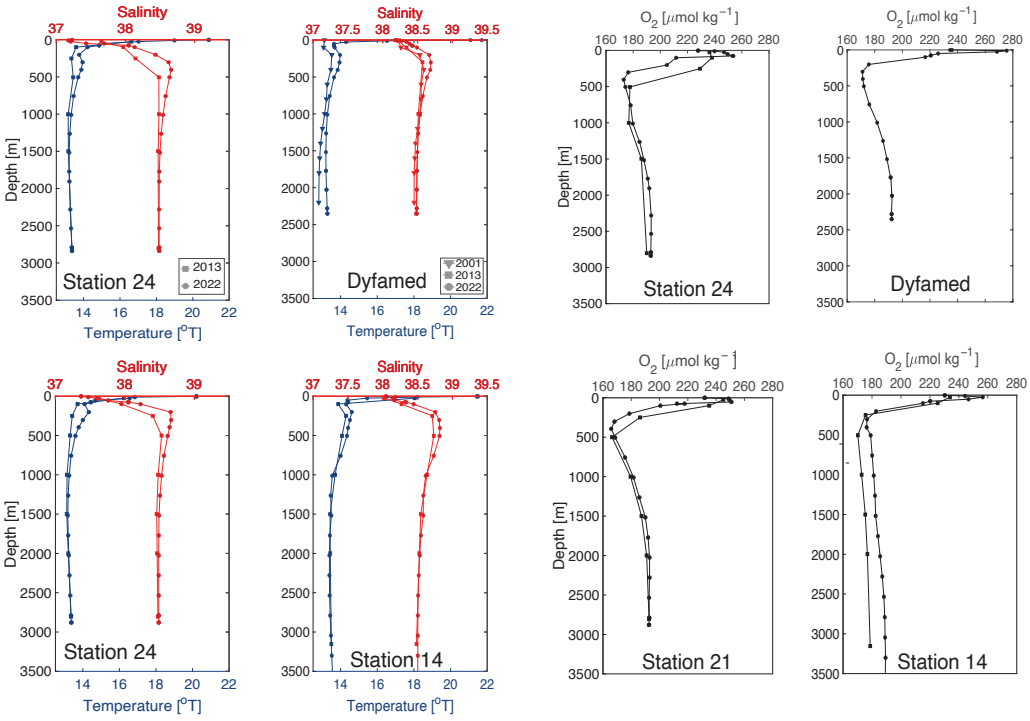

Figure A1. Comparison of Salinity (red), Temperature (blue) and Dissolved Oxygen (black) data from 2013 and 2022 along four stations in the Western Mediterranean Sea.

Table A1. Parameter ranges used in this study to distinguish different water masses. We here report also the references where these ranges where originally defined.

Water Mass	Abbreviation	Pot. Temp °C	Salinity	Oxygen µmol kg^{-1}	Reference
Atlantic Water	AW	>14, 16.4	>36.5 Algero-Provençal: 38–38.3	>230	[8,38,49]
Levantine Intermediate Water (east)	LIW	>13.5	>38.47	>164	[8,38,39,49]
Western Intermediate Water	WIW	12.0–13.0	38-38.3		[8]
West Medit. Deep Water-new	WMDWn	12.90	38.485	185	[38]
West Medit. Deep Water-old	WMDWo	12.87, 12.75–12.8	38.44–38.46	179	[11,38]
West Medit. Deep water	WMDW	12.8–12.9	38.4–38.45	195–205	[39]
Tyrrhenian Dense Water	TDW	12.85	38.46		[8]

Table A2. Data of temperature, salinity, oxygen, ^{236}U, ^{238}U,$^{236}U/^{238}U$ ratio and ^{129}I of single stations collected in the *TAlPro2022* expedition. Each seawater sample is assigned to a water mass. The reported uncertainties for the radionuclide concentrations are based on internal standard replicates for ^{129}I and total propagated uncertainty for ^{236}U. Bad quality data for ^{129}I (excluded from Results and Discussion) is marked here with "*".

Station	Depth m	Water Mass	Salinity	Pot. Temp °C	Oxygen µmol kg^{-1}	^{236}U Concentration 10^6 at kg^{-1}			^{238}U Concentration µg kg^{-1}			$^{236}U/^{238}U$ 10^{-12} at kg^{-1}			^{129}I Concentration 10^7at kg^{-1}		
Station 21	1	surface	37.37	20.22	231.75	13.47	±	0.33	3.56	±	0.09	1493	±	52	11.54	±	0.55
Algero-Provençal Basin	26	AW	37.60	16.55	249.43	14.75	±	0.29	3.70	±	0.06	1576	±	41	13.25	±	0.63
38.5988°	54	AW	37.76	14.68	250.82	15.66	±	0.39	3.71	±	0.07	1668	±	53	12.05	±	0.57
5.5982°	100	AW/LIW	38.22	14.08	200.55	18.70	±	0.34	3.63	±	0.06	2035	±	49	13.10	±	0.62
date: 23 May 2022	200	LIW	38.66	14.30	178.66	16.28	±	0.33	3.52	±	0.05	1828	±	46	12.01	±	0.57
	300	LIW	38.67	13.96	168.12	18.26	±	0.41	4.01	±	0.08	1800	±	54	12.01	±	0.58
	500	LIW/WMDW	38.62	13.52	168.62	13.96	±	0.29	3.76	±	0.09	1466	±	46	9.97	±	0.47
	750	WMDW	38.56	13.25	175.61	12.84	±	0.30	3.77	±	0.08	1346	±	42	9.79	±	0.47
	1000	WMDW	38.53	13.10	181.56	12.08	±	0.34	3.75	±	0.09	1275	±	47	7.80	±	0.37
	1250	WMDW	38.51	13.01	185.71	11.94	±	0.33	3.73	±	0.10	1265	±	48	* 12.51	±	0.59
	1500	WMDW	38.49	12.95	189.96	12.98	±	0.34	3.83	±	0.08	1340	±	45	8.71	±	0.42
	1750	WMDW	38.49	12.93	191.91	13.50	±	0.39	3.63	±	0.07	1468	±	51	* 4.29	±	0.21
	2000	WMDW	38.49	12.92	192.92	14.56	±	0.52	3.45	±	0.06	1667	±	67	9.34	±	0.44
	2250	WMDW	38.49	12.92	192.96	13.90	±	0.63	3.41	±	0.05	1610	±	78	8.68	±	0.41
	2500	WMDW	38.49	12.92	192.59	12.86	±	0.38	3.61	±	0.07	1408	±	51	9.43	±	0.45
	2750	WMDW	38.49	12.92	192.63	13.04	±	0.40	3.63	±	0.07	1421	±	51	9.11	±	0.43
	2838	WMDW	38.49	12.92	192.45	14.27	±	0.85	3.75	±	0.09	1505	±	98	11.79	±	0.55
Station 24	2	surface	37.23	20.87	228.00	12.36	±	0.41	3.38	±	0.05	1446	±	53	9.82	±	0.47
Algero-Provençal Basin	25	AW	37.21	17.02	246.96	12.33	±	0.36	3.47	±	0.07	1405	±	49	12.51	±	0.60
40.2007°	50	AW	37.43	15.12	249.46	13.88	±	0.39	3.43	±	0.06	1598	±	52	15.81	±	0.75
5.4998	100	WIW/LIW	38.13	14.20	211.64	17.89	±	0.32	3.66	±	0.05	1930	±	45	14.22	±	0.67
date: 24 May 2022	201	WIW/LIW	38.44	13.73	204.75	17.86	±	0.32	3.72	±	0.07	1900	±	49	15.21	±	0.72
	300	LIW	38.62	13.90	176.36	15.85	±	0.35	3.65	±	0.07	1717	±	51	11.82	±	0.57
	501	LIW/WMDW	38.64	13.63	174.27	14.55	±	0.32	3.73	±	0.06	1540	±	42	9.50	±	0.45
	751	WMDW	38.58	13.34	178.13	13.06	±	0.28	3.70	±	0.07	1394	±	40	8.81	±	0.42
	1000	WMDW	38.54	13.17	179.72	12.02	±	0.25	3.75	±	0.09	1267	±	60	7.71	±	0.37
	1251	WMDW	38.52	13.05	184.71	12.33	±	0.25	3.73	±	0.08	1308	±	40	9.53	±	0.46
	1500	WMDW	38.50	12.98	187.98	12.53	±	0.25	3.57	±	0.05	1387	±	35	8.05	±	0.38
	1751	WMDW	38.49	12.94	190.74	12.63	±	0.36	3.68	±	0.07	1358	±	47	9.48	±	0.45
	1883	WMDW	38.49	12.93	191.87	12.58	±	0.28	3.76	±	0.06	1320	±	36	8.60	±	0.41
	2251	WMDW	38.49	12.92	193.26	12.86	±	0.34	3.65	±	0.08	1392	±	47	10.53	±	0.50
	2500	WMDW	38.49	12.92	193.23	13.69	±	0.29	3.50	±	0.05	1548	±	40	11.76	±	0.56
	2751	WMDW	38.49	12.92	193.16	13.54	±	0.27	3.49	±	0.05	1531	±	38	13.38	±	0.64
	2799	WMDW	38.49	12.92	192.97	13.04	±	0.36	3.70	±	0.10	1392	±	55	8.84	±	0.43

Table A2. *Cont.*

Station	Depth m	Water Mass	Salinity	Pot. Temp °C	Oxygen µmol kg^{-1}	^{236}U Concentration 10^6 at kg^{-1}			^{238}U Concentration µg kg^{-1}			^{236}U/^{238}U 10^{-12} at kg^{-1}			^{129}I Concentration 10^7at kg^{-1}		
Station DYFAMED	1	surface	38.18	21.08	235.99	16.35	±	0.58	3.48	±	0.07	1858	±	76	15.67	±	0.75
Ligurian Sea	26	AW	38.34	14.29	268.53	17.29	±	0.63	3.53	±	0.10	1934	±	89	13.41	±	0.64
43.4180°	50	AW	38.39	13.64	225.86	17.79	±	0.76	3.55	±	0.08	1983	±	97	13.42	±	0.65
7.8683°	100	AW/LIW	38.49	13.66	216.54	17.13	±	0.55	3.61	±	0.07	1877	±	71	12.17	±	0.58
date: 25 May 2022	200	LIW	38.67	13.94	175.69	16.73	±	0.49	3.54	±	0.06	1868	±	62	12.72	±	0.61
	300	LIW	38.69	13.90	171.13	15.16	±	0.40	3.65	±	0.07	1640	±	54	12.05	±	0.58
	401	LIW	38.68	13.78	171.37	14.73	±	0.64	3.59	±	0.07	1622	±	77	* 16.65	±	0.79
	500	WMDW	38.63	13.57	172.07	13.83	±	0.63	3.66	±	0.07	1495	±	75	9.93	±	0.48
	751	WMDW	38.57	13.30	176.07	12.78	±	0.40	3.69	±	0.07	1369	±	51	* 13.68	±	0.65
	1001	WMDW	38.53	13.13	181.79	12.09	±	0.28	3.60	±	0.07	1328	±	41	8.77	±	0.42
	1250	WMDW	38.51	13.03	185.98	13.18	±	0.69	3.52	±	0.06	1481	±	82	* 12.93	±	0.62
	1501	WMDW	38.50	12.97	188.90	11.79	±	0.36	3.58	±	0.07	1303	±	46	8.57	±	0.43
	1750	WMDW	38.49	12.94	191.40	12.35	±	0.40	3.58	±	0.07	1363	±	52	8.73	±	0.44
	2001	WMDW	38.49	12.92	192.58	12.55	±	0.46	3.59	±	0.07	1381	±	57	9.67	±	0.47
	2250	WMDW	38.49	12.92	192.37	13.02	±	0.31	3.52	±	0.07	1460	±	45	* 14.49	±	0.70
	2319	WMDW	38.49	12.92	192.26	12.79	±	0.33	3.54	±	0.07	1428	±	45	10.54	±	0.50
Station 14	1	surface	38.05	21.43	230.43	16.19	±	0.44	3.67	±	0.10	1743	±	67	13.88	±	0.66
Tyrrhenian Sea	24	AW	38.14	15.45	256.50	16.74	±	0.44	3.58	±	0.11	1848	±	74	11.80	±	0.56
39.7197°	50	AW	38.17	14.37	246.66	16.86	±	0.48	3.70	±	0.11	1801	±	74	12.52	±	0.60
11.8708°	101	AW/LIW	38.44	14.28	215.16	16.30	±	0.40	3.50	±	0.07	1841	±	57	11.19	±	0.53
date: 20 May 2022	200	LIW	38.75	14.58	182.82	17.02	±	0.52	3.69	±	0.12	1825	±	82	13.18	±	0.62
	301	LIW	38.81	14.46	176.55	16.04	±	0.56	3.59	±	0.09	1768	±	76	12.47	±	0.59
	500	LIW	38.82	14.27	179.07	15.41	±	0.46	3.52	±	0.08	1728	±	65	11.30	±	0.54
	751	tEMDW/LIW	38.73	13.89	180.11	13.66	±	0.49	3.72	±	0.15	1452	±	79	9.26	±	0.45
	1001	tEMDW	38.62	13.40	181.18	12.35	±	0.35	3.71	±	0.10	1316	±	51	8.62	±	0.42
	1250	tEMDW	38.58	13.27	182.10	11.52	±	0.38	3.76	±	0.06	1211	±	45	9.13	±	0.44
	1500	tEMDW	38.58	13.26	182.52	11.35	±	0.43	3.77	±	0.08	1190	±	52	7.16	±	0.35
	1751	tEMDW/TDW	38.55	13.14	184.08	10.84	±	0.59	3.55	±	0.07	1207	±	69	7.43	±	0.36
	2000	tEMDW/TDW	38.53	13.08	185.65	12.26	±	0.49	3.62	±	0.11	1340	±	67	8.12	±	0.39
	2250	TDW	38.52	13.04	187.08	11.77	±	0.35	3.53	±	0.07	1317	±	47	7.44	±	0.36
	2501	TDW	38.51	13.01	188.20	11.87	±	0.33	3.63	±	0.10	1292	±	51	9.56	±	0.46
	2750	TDW	38.50	12.99	188.83	12.65	±	0.29	3.69	±	0.10	1355	±	49	8.90	±	0.43
	3001	TDW	38.50	12.99	189.05	12.53	±	0.33	3.60	±	0.14	1376	±	63	8.49	±	0.41
	3250	TDW	38.50	12.99	189.36	11.93	±	0.34	3.72	±	0.08	1268	±	45	8.42	±	0.42
	3481	TDW	38.50	12.99	189.10	12.48	±	0.31	3.67	±	0.08	1346	±	45	8.61	±	0.42

Table A3. Values of ^{129}I gaseous release for calculation of required atmospheric input to justify the surface inventory of ^{129}I in the Algero-Provençal (AP) Basin. Data of gaseous releases were obtained from https://cdn.orano.group/orano/docs/default-source/orano-doc/groupe/publications-reference/environnement-edition-2023.pdf?sfvrsn=2f8da5a_10 (accessed on 3 November 2024; Orano La Hague) and https://www.gov.uk/government/publications/radioactivity-in-food-and-the-environment-rife-reports/rife-28-radioactivity-in-food-and-the-environment-2022 (accessed on 3 November 2024; UK Government for Sellafield).

	Gaseous Release Bq	Total Release Bq	Total Release at	Surface Inventory AP Basin at m^{-2}	Surface Area km^2	Surface Inventory AP Basin at
La Hague	4.7×10^9	6.5×10^9	4.6×10^{24}	5.3×10^{12}	35,500	1.9×10^{23}
Sellafield	1.8×10^9					

References

1. Talley, L.D.; Pickard, G.L.; Emery, W.J.; Swift, J.H. Chapter 1—Introduction to Descriptive Physical Oceanography. In *Descriptive Physical Oceanography*, 6th ed.; Talley, L.D., Pickard, G.L., Emery, W.J., Swift, J.H., Eds.; Academic Press: Boston, MA, USA, 2011; pp. 1–6. [CrossRef]
2. Millot, C. Circulation in the Mediterranean Sea: Evidences, debates and unanswered questions. *Sci. Mar.* **2005**, *69*, 5–21. [CrossRef]
3. Talley, L.D.; Pickard, G.L.; Emery, W.J.; Swift, J.H. Chapter 5—Mass, Salt, and Heat Budgets and Wind Forcing. In *Descriptive Physical Oceanography*, 6th ed.; Talley, L.D., Pickard, G.L., Emery, W.J., Swift, J.H., Eds.; Academic Press: Boston, MA, USA, 2011; pp. 111–145. [CrossRef]
4. Durrieu de Madron, X.; Guieu, C.; Sempéré, R.; Conan, P.; Cossa, D.; D'Ortenzio, F.; Estournel, C.; Gazeau, F.; Rabouille, C.; Stemmann, L.; et al. Marine ecosystems' responses to climatic and anthropogenic forcings in the Mediterranean. *Prog. Oceanogr.* **2011**, *91*, 97–166. [CrossRef]
5. Vargas-Yáñez, M.; García-Martínez, M.C.; Moya, F.; Balbín, R.; López-Jurado, J.L.; Serra, M.; Zunino, P.; Pascual, J.; Salat, J. Updating temperature and salinity mean values and trends in the Western Mediterranean: The RADMED project. *Prog. Oceanogr.* **2017**, *157*, 27–46. [CrossRef]
6. Tanhua, T.; Hainbucher, D.; Schröder, K.; Cardin, V.; Álvarez, M.; Civitarese, G. The Mediterranean Sea system: A review and an introduction to the special issue. *Ocean. Sci.* **2013**, *9*, 789–803. [CrossRef]
7. Robinson, A.R.; Leslie, W.G.; Theocharis, A.; Lascaratos, A. Mediterranean sea circulation. *Ocean. Curr.* **2001**, *1*, 283–298.
8. Schroeder, K.; Garcìa-Lafuente, J.; Josey, S.A.; Artale, V.; Nardelli, B.B.; Carrillo, A.; Gacic, M.; Gasparini, G.P.; Herrmann, M.; Lionello, P.; et al. Circulation of the Mediterranean Sea and its variability. In *The Climate of the Mediterranean Region: From the Past to the Future* ; Elsevier: Amsterdam, The Netherlands, 2012; pp. 187–256.
9. Schroeder, K.; Chiggiato, J.; Bryden, H.; Borghini, M.; Ben Ismail, S. Abrupt climate shift in the Western Mediterranean Sea. *Sci. Rep.* **2016**, *6*, 23009. [CrossRef]
10. Schröder, K.; Ribotti, A.; Borghini, M.; Sorgente, R.; Perilli, A.; Gasparini, G.P. An extensive western Mediterranean deep water renewal between 2004 and 2006. *Geophys. Res. Lett.* **2008**, *35*, 1–7. [CrossRef]
11. Schröder, K.; Gasparini, G.P.; Tangherlini, M.; Astraldi, M. Deep and intermediate water in the western Mediterranean under the influence of the Eastern Mediterranean Transient. *Geophys. Res. Lett.* **2006**, *33*, 1–6. [CrossRef]
12. Roether, W.; Manca, B.; Klein, B.; Bregant, D.; Georgopoulos, D.; Beitzel, V.; Kovacevic, V.; Luchetta, A. Recent Changes in Eastern Mediterranean Deep Waters. *Science* **1996**, *271*, 333–335. [CrossRef]
13. Fine, R.A. Observations of CFCs and SF6 as Ocean Tracers. *Annu. Rev. Mar. Sci.* **2011**, *3*, 173–195. [CrossRef]
14. Casacuberta, N.; Smith, J.N. Nuclear Reprocessing Tracers Illuminate Flow Features and Connectivity Between the Arctic and Subpolar North Atlantic Oceans. *Annu. Rev. Mar. Sci.* **2023**, *15*, 203–221. [CrossRef] [PubMed]
15. Smith, J.N.; McLaughlin, F.A.; Smethie, W.M., Jr.; Moran, S.B.; Lepore, K. Iodine-129, 137Cs, and CFC-11 tracer transit time distributions in the Arctic Ocean. *J. Geophys. Res. Ocean.* **2011**, *116*, 1–19. [CrossRef]
16. Snyder, G.; Aldahan, A.; Possnert, G. Global distribution and long-term fate of anthropogenic 129I in marine and surface water reservoirs. *Geochem. Geophys. Geosyst.* **2010**, *11*, Q04010. [CrossRef]
17. Raisbeck, G.; Yiou, F. 129I in the oceans: Origins and applications. *Sci. Total Environ.* **1999**, *237–238*, 31–41. [CrossRef] [PubMed]
18. Christl, M.; Casacuberta, N.; Lachner, J.; Maxeiner, S.; Vockenhuber, C.; Synal, H.A.; Goroncy, I.; Herrmann, J.; Daraoui, A.; Walther, C.; et al. Status of 236U analyses at ETH Zurich and the distribution of 236U and 129I in the North Sea in 2009. *Nucl. Instrum. Methods Phys. Res. Sect. Beam Interact. Mater. Atoms* **2015**, *361*, 510–516. [CrossRef]
19. Sakaguchi, A.; Kawai, K.; Steier, P.; Quinto, F.; Mino, K.; Tomita, J.; Hoshi, M.; Whitehead, N.; Yamamoto, M. First results on 236U levels in global fallout. *Sci. Total Environ.* **2009**, *407*, 4238–4242. [CrossRef]
20. Christl, M.; Casacuberta, N.; Vockenhuber, C.; Elsässer, C.; Bailly Du Bois, P.; Herrmann, J.; Synal, H.A. Reconstruction of the 236U input function for the Northeast Atlantic Ocean: Implications for 129I/236U and 236U/238U-based tracer ages. *J. Geophys. Res. Ocean.* **2015**, *120*, 7282–7299. [CrossRef]

21. Herbert Reithmeier, H.; Vitali Lazarev, V.; Rühm, W.; Schwikowski, M.; Gaeggeler, H.; Nolte, E. Estimate of European 129I Releases Supported by 129I Analysis in an Alpine Ice Core. *Environ. Sci. Technol.* **2006**, *40*, 5891–5896. [CrossRef]
22. Dale, D.; Christl, M.; Vockenhuber, C.; Macrander, A.; Ólafsdóttir, S.; Middag, R.; Casacuberta, N. Tracing ocean circulation and mixing from the Arctic to the subpolar North Atlantic using the 129I–236U dual tracer. *J. Geophys. Res. Ocean.* **2024**, *129*, e2024JC021211. [CrossRef]
23. Payne, A.; Wefing, A.M.; Christl, M.; Vockenhuber, C.; Williams, W.; Smith, J.N.; Casacuberta, N. Circulation Timescales and Pathways of Atlantic Water in the Canada Basin: Insights From Transient Tracers 129I and 236U. *J. Geophys. Res. Ocean.* **2024**, *129*, e2023JC020813. [CrossRef]
24. Castrillejo, M.; Casacuberta, N.; Christl, M.; Garcia-Orellana, J.; Vockenhuber, C.; Synal, H.A.; Masqué, P. Anthropogenic 236U and 129I in the Mediterranean Sea: First comprehensive distribution and constrain of their sources. *Sci. Total Environ.* **2017**, *593–594*, 745–759. [CrossRef] [PubMed]
25. López-Lora, M.; Chamizo, E.; Levy, I.; Christl, M.; Casacuberta, N.; Kenna, T.C. 236U, 237Np and 239,240Pu as complementary fingerprints of radioactiveeffluents in the western Mediterranean Sea and in the Canada Basin (Arctic Ocean). *Sci. Total Environ.* **2021**, *765*, 142741. [CrossRef]
26. Chamizo, E.; López-Lora, M.; Bressac, M.; Levy, I.; Pham, M.K. Excess of 236U in the northwest Mediterranean Sea. *Sci. Total Environ.* **2016**, *565*, 767–776. [CrossRef] [PubMed]
27. Yiou, F.; Raisbeck, G.; Zhou, Z.; Kilius, L. *129I in the Mediterranean Sea*; Les Editions de Physique: Paris, France, 1997.
28. Zhao, X.; Kieser, W.; Litherland, A.; Smith, J.; Fowler, S.; Miquel, J. *The AMS Analysis of 129I and 135Cs: Development of Tools for Oceanographic Tracing and Pollution Source Identification*; Technical Report 1011–4289; International Atomic Energy Agency (IAEA): Vienna, Austria, 1999.
29. Hou, X.; Hansen, V.; Aldahan, A.; Possnert, G.; Lind, O.C.; Lujaniene, G. A review on speciation of iodine-129 in the environmental and biological samples. *Anal. Chim. Acta* **2009**, *632*, 181–196. [CrossRef] [PubMed]
30. Talerko, M.; Garger, E.; Lev, T.; Nosovskyi, A. Atmospheric transport of radionuclides initially released as a result of the Chernobyl accident. In *Behavior of Radionuclides in the Environment II: Chernobyl*; Springer: Singapore, 2020; pp. 3–74.
31. Schroeder, K.; Tanhua, T.; Bryden, H.L.; Álvarez, M.; Chiggiato, J.; Aracri, S. Mediterranean sea ship-based hydrographic investigations program (Med-SHIP). *Oceanography* **2015**, *28*, 12–15. [CrossRef]
32. Casacuberta, N.; Masqué, P.; Henderson, G.; Rutgers van-der Loeff, M.; Bauch, D.; Vockenhuber, C.; Daraoui, A.; Walther, C.; Synal, H.A.; Christl, M. First 236U data from the Arctic Ocean and use of 236U/238U and 129I/236U as a new dual tracer. *Earth Planet. Sci. Lett.* **2016**, *440*, 127–134. [CrossRef]
33. Wefing, A.M.; Christl, M.; Vockenhuber, C.; Rutgers van der Loeff, M.; Casacuberta, N. Tracing Atlantic Waters Using 129I and 236U in the Fram Strait in 2016. *J. Geophys. Res. Ocean.* **2019**, *124*, 882–896. [CrossRef]
34. Christl, M.; Lachner, J.; Vockenhuber, C.; Goroncy, I.; Herrmann, J.; Synal, H.A. First data of Uranium-236 in the North Sea. *Nucl. Instruments Methods Phys. Res. Sect. Beam Interact. Mater. Atoms* **2013**, *294*, 530–536. [CrossRef]
35. Christl, M.; Gautschi, P.; Maxeiner, S.; Müller, A.M.; Vockenhuber, C.; Synal, H.A. 236U analyses with the ETH Zurich MILEA prototype system. *Nucl. Instrum. Methods Phys. Res. Sect. Beam Interact. Mater. Atoms* **2023**, *534*, 61–71. [CrossRef]
36. Wefing, A.M. 129I and 236U as a New Tracer Pair to Study Water Mass Circulation in the Arctic Ocean and Fram Strait. Ph.D. Thesis, ETH Zurich, Zurich, Switzerland, 2021.
37. Pates, J.M.; Muir, G.K.P. U–salinity relationships in the Mediterranean: Implications for 234Th:238U particle flux studies. *Mar. Chem.* **2007**, *106*, 530–545. [CrossRef]
38. Hainbucher, D.; Rubino, A.; Cardin, V.; Tanhua, T.; Schröder, K.; Bensi, M. Hydrographic situation during cruise M84/3 and P414 (spring 2011) in the Mediterranean Sea. *Ocean. Sci.* **2014**, *10*, 669–682. [CrossRef]
39. Mavropoulou, A.M.; Vervatis, V.; Sofianos, S. Dissolved oxygen variability in the Mediterranean Sea. *J. Mar. Syst.* **2020**, *208*, 103348. [CrossRef]
40. Chamizo, E.; Christl, M.; López-Lora, M.; Casacuberta, N.; Wefing, A.M.; Kenna, T.C. The potential of 233U/236U as a water mass tracer in the Arctic Ocean. *J. Geophys. Res. Ocean.* **2022**, *127*, e2021JC017790. [CrossRef]
41. Li, P.; Tanhua, T. Recent Changes in Deep Ventilation of the Mediterranean Sea; Evidence From Long-Term Transient Tracer Observations. *Front. Mar. Sci.* **2020**, *7*, 1–23. [CrossRef]
42. Margirier, F.; Testor, P.; Heslop, E.; Mallil, K.; Bosse, A.; Houpert, L.; Mortier, L.; Bouin, M.N.; Coppola, L.; D'Ortenzio, F.; et al. Abrupt warming and salinification of intermediate waters interplays with decline of deep convection in the Northwestern Mediterranean Sea. *Sci. Rep.* **2020**, *10*, 20923. [CrossRef]
43. Roether, W.; Jean-Baptiste, P.; Fourré, E.; Sültenfuß, J. The transient distributions of nuclear weapon-generated tritium and its decay product 3 He in the Mediterranean Sea, 1952–2011. and their oceanographic potential. *Ocean. Sci.* **2013**, *9*, 837–854. [CrossRef]
44. Delfanti, R.; Papucci, C. Mediterranean Sea: Radionuclides. In *Encyclopedia of Inorganic Chemistry*; John Wiley & Sons, Ltd.: New York, NY, USA, 2006.
45. Stöven, T.; Tanhua, T. Ventilation of the Mediterranean Sea constrained by multiple transient tracer measurements. *Ocean. Sci.* **2014**, *10*, 439–457. [CrossRef]
46. Schneider, A.; Tanhua, T.; Roether, W.; Steinfeldt, R. Changes in ventilation of the Mediterranean Sea during the past 25 year. *Ocean. Sci.* **2014**, *10*, 1–16. [CrossRef]

47. Osterc, A.; Stibilj, V. Influence of releases of I-129 from reprocessing plants on the marine environment of the North Adriatic Sea. *Chemosphere* **2012**, *86*, 1020–1027. [CrossRef]
48. Gómez-Guzmán, J.M.; Enamorado-Báez, S.M.; Pinto-Gómez, A.R.; Abril-Hernández, J.M.; López-Gutiérrez, J.M.; García-León, M. Anthropogenic 129I concentration and 129I/127I ratio in rainwater from Seville (Spain) in the period 2005–2008 as affected by airborne releases from Sellafield and La Hague facilities. *Atmos. Environ.* **2012**, *56*, 26–32. [CrossRef]
49. Millot, C. Circulation in the Western Mediterranean Sea. *J. Mar. Syst.* **1999**, *20*, 423–442. [CrossRef]